Journal of Computational Physics 236 (2013) 493–512

Contents lists available at SciVerse ScienceDirect

Journal of Computational Physics

journal homepage: www.elsevier.com/locate/jcp

A dispersively accurate compact finite difference method for the Degasperis–Procesi equation

C.H. Yu [a], Tony W.H. Sheu [a,b,c,*]

[a] Department of Engineering Science and Ocean Engineering, National Taiwan University, Taipei, Taiwan, ROC
[b] Department of Mathematics, National Taiwan University, Taipei, Taiwan, ROC
[c] Center of Advanced Study in Theoretical Sciences (CASTS), National Taiwan University, Taipei, Taiwan, ROC

ARTICLE INFO

Article history:
Received 15 November 2011
Received in revised form 31 August 2012
Accepted 27 October 2012
Available online 29 November 2012

Keywords:
Non-dissipative
Degasperis–Procesi equation
Shockpeakon
Symplecticity-preserving
Conservation of Hamiltonians

ABSTRACT

In this paper we are aimed to solve the non-dissipative Degasperis–Procesi equation based on the $u - P$ formulation. To resolve the computational difficulty at the wave crest where the first-order derivative may diverge and the shockpeakon solution may form, the first-order spatial derivative term in the two-step equations will be approximated in a conservative form. The resulting equations will be approximated by the symplecticity-preserving time-stepping scheme and the spatial discretization scheme that can optimize the numerical wavenumber for the first-order spatial derivative term. This scheme will be developed in a three-point grid stencil with the accuracy order of seventh within the combined compact finite difference framework. Besides the validation of numerical accuracy, we will in particular address the discrete conservation of Hamiltonians even when peakon collides with antipeakon and generates, as a result, a shockpeakon. We will also demonstrate the capability of applying the proposed numerical method to sharply resolve some important features of the third-order dispersive DP equation.

1. Introduction

Many existing third-order nonlinear partial differential equations in the areas of hydraulics and optics permit formation of soliton solutions. Soliton is by definition a solitary wave (or a humped wave of budge of water). When a soliton nonlinearly interacts with the other soliton waves, both wave velocity and shape can be asymptotically preserved. In this class of equations, the most distinguished equation bears the names of Korteweg and de Vries (KdV). KdV equation models the time-evolving wave in a single direction and has two competing terms. One is the nonlinear advective term uu_x that can cause a steepening of wave to occur and the other nonlinear dispersion term uu_{xxx} is responsible for the spreading of wave. Formation of solitons in KdV equation is the result of a delicate balance of the narrowing effect due to convective nonlinearity and the widening effect due to the dispersion in the medium. While KdV equation has many remarkable properties, this equation has, for example, the non-physically unbounded dispersion relation. The Benjamin–Bona–Mahony (BBM) equation, introduced as one of the alternatives to the KdV equation, replaces the linear dispersion term u_{xxx} with the mixed derivative term $-u_{xxt}$. This replacement of the differential term results in a desirable bounded dispersion relation and helps to get some theoretical aspects such as the solution existence, uniqueness, and regularity [1].

* Corresponding author at: Department of Engineering Science and Ocean Engineering, National Taiwan University, Taipei, Taiwan, ROC. Tel.: +886 2 33665746; fax: +886 2 23929885.
E-mail address: twhsheu@ntu.edu.tw (T.W.H. Sheu).

0021-9991/$ - see front matter © 2012 Elsevier Inc. All rights reserved.
http://dx.doi.org/10.1016/j.jcp.2012.10.046

Besides the nonlinear steepening term uu_x shown in the KdV and BBM equations, the so-called Camassa–Holm (CH) equation contains one additional dispersion term uu_{xxx}. This nonlinear dispersion term is in contrast to the linear dispersion term u_{xxx} in KdV equation and the linear dispersion term $-u_{xxt}$ in BBM equation. CH equation derived from the asymptotic expansion of the incompressible Euler equations in shallow water regime is bi-Hamiltonian [2]. Like the KdV equation, the CH equation can be completely integrable and has therefore an infinite number of conservation laws. This equation permits also the solution of a soliton type in the non-zero case of linear dispersion. In the absence of this linear dispersion term, CH equation is amenable to peakon solution, which has jumps in its derivative but not in the solution itself.

Degasperis–Procesi (DP) equation has a strong similarity to CH equation in the sense that they all belong to the b-family of the integrable equations given by $u_t - u_{xxt} + (b+1)uu_x = bu_xu_{xx} + uu_{xxx}$. The CH and DP equations correspond to $b = 2$, $b = 3$, respectively. Besides the peaked solitary wave solutions (or peakons), DP equation admits also the cuspon solution. The traveling wave solutions for the CH and DP equations are smooth except at the wave crest, at which the spatial derivative of the wave solution changes sign. This means that peakons have finite jumps in the first derivative of the solution. Cuspon is known as the other form of the solitons where its solution exhibits cusps at the wave crest. Unlike the peakon solutions where the derivatives differ only by a sign at the wave peak, at the jump of cuspon the derivatives diverge.

Despite many similarities, the invariants and the bi-Hamiltonian structures in CH and DP equations are substantially different. Besides, the solution nature of the DP equation differs from that of the CH equation. One of the major differences between the two completely integrable equations is that DP equation permits not only the peakon solution given by $u(x,t) = ce^{-|x-ct|}$ [3] but is also amenable to the shock solution $-\frac{1}{t+c}sign(x)e^{-|x|}(c>0)$ [4,5]. Besides the solution discontinuity occurring possibly in the DP equation but not at all in the CH equation, the conservation laws embedded in the DP equation are much weaker than those in the CH equation [6]. When peakons and antipeakons appear simultaneously in the solution domain, the issue being referred to as the wave collision may be present. Subsequent to a wave collision, by now the solution of CH equation is well understood in comparison with that in the DP equation [5]. For this reason, how to numerically capture shocks in DP equation will be particularly addressed. In addition, both wave propagation scenario and Hamiltonian-preserving nature after a peakon–antipeakon collision will be explored.

In comparison with the CH equation that permits only the peakon solution, the third-order nonlinear dispersive DP equation supports peakon as well as shock solutions. The increasingly deteriorated smoothness in the DP solution makes the numerical analysis of this equation an even difficult task than the calculation of CH equation. One can find only few numerical studies of DP equation in the literature. Entropy weak solution to DP equation has been predicted by Coclite et al. [7] and Feng and Liu [8] by the operator splitting schemes of different kinds. Hoel [9] has captured multi-shockpeakons by applying the particle method to solve the DP equation. Note that the above three numerical methods in [7–9] were developed mainly for the purpose of capturing shock solutions. They had no intension to conserve the invariants in their scheme development for the DP equation. After solving the KdV equation [10] and then the CH equation [11], Xu and Shu applied further the time-dependent discontinuous Galerkin method detailed in [12] to resolve shockpeakon discontinuity in the DP equation [6]. More recently, on the basis of bi-Hamiltonian structure Miyatake and Matsuo [13] proposed two conservative finite difference schemes to preserve two invariants $H_{-1}(\equiv -\frac{1}{6}u^3)$ and $H_0(\equiv -\frac{9}{2}(u-u_{xx}))$ for the DP equation with sufficiently smooth solutions.

This paper is organized as follows. In Section 2, some of the distinguished features in the DP equation which are the useful ingredients to be applied to develop the proposed scheme for the highly dispersive working equation are summarized. Section 3 contains the employed two-step $u-P$ formulation. In Section 4, we will detail the development of the proposed symplecticity-preserving time-stepping scheme and then present the three-point seventh-order accurate scheme, which optimizes also the numerical wavenumber, for the first-order spatial derivative term. Numerical results will be presented in Section 5 to demonstrate the ability of yielding a better prediction accuracy and the capability of preserving symplectic geometric structure and the discrete conservation laws for the current investigated non-dissipative differential system. The scheme capability of resolving shockpeakons will be also numerically demonstrated. Concluding remarks will be given in Section 6.

2. Working equation and its fundamentals

Subject to an initial condition, the following DP equation will be solved in a domain with the periodic condition specified at the two truncated ends

$$u_t - u_{xxt} + 3\kappa^3 u_x + 4uu_x - uu_{xxx} - 3u_xu_{xx} = 0. \tag{1}$$

The above equation is considered as an approximation to the incompressible Euler equations for the modeling of shallow water propagation in conditions of small amplitude and long wavelength. The solution $u(x,t)$ to Eq. (1) denotes the horizontal component of fluid velocity at time t in the x-direction. In the family of the third-order partial differential equation given by $u_t + c_0u_x + \gamma u_{xxx} - \epsilon^2 u_{xxt} = (c_1u^2 + c_2u_x^2 + c_3uu_{xx})_x$, only the KdV equation ($\epsilon = c_2 = c_3 = 0$), CH equation ($c_1 = -\frac{3c_3}{2\epsilon^2},\ c_2 = \frac{c_3}{2}$), and DP equation ($c_1 = -\frac{2c_3}{\epsilon^2},\ c_2 = c_3$) satisfy the asymptotic integrability condition [6].

In the absence of a linear advection term, the resulting highly nonlinear and non-dissipative DP equation (1) admits the Lax pair given below for the differential system involving the eigenfunction ψ and its associated eigenvalue λ [3].

$$\psi_x - \psi_{xxx} = \lambda(u - u_{xx})\psi, \tag{2}$$

$$\psi_t + \frac{1}{\lambda}\psi_{xx} + u\psi_x - \left(u_x + \frac{2}{3\lambda}\right)\psi = 0. \tag{3}$$

Because of the existence of Lax pair, the dispersive equation (1) is completely integrable. In comparison with the second-order self-adjoint differential operator in CH equation, the non-selfadjoint third-order differential operator in (2) makes the integrable structure in Eq. (1) more complex than the CH equation [14].

The nonlinear equation (1) under current investigation can be rewritten in its equivalent Hamiltonian form. For the evolution of the momentum variable defined by $m = u - u_{xx}$, two equations for $m_t(\equiv \frac{\partial m}{\partial t})$ can be derived as follows [15]

$$m_t = B_0 \frac{\delta H_{-1}}{\delta m} = B_1 \frac{\delta H_0}{\delta m}. \tag{4}$$

In the above, $H_0(\equiv -\frac{9}{2}\int m dx)$ and $H_{-1}(\equiv -\frac{1}{6}\int u^3 dx)$ are the Hamiltonians corresponding to the respective skew-symmetric operators $B_0(\equiv \partial x(1-\partial_x^2)(4-\partial_x^2))$ and $B_1(\equiv m^{2/3}\partial_x m^{1/3}(\partial_x - \partial_x^3)^{-1} m^{1/3}\partial_x m^{2/3})$. Thanks to the compatible bi-Hamiltonian pair in (4), DP equation has a bi-Hamiltonian structure. How to incorporate this salient Hamiltonian feature of the DP equation into the numerical framework plays a key role to get a long-term physically accurate DP solution. Note that the conservative scheme for DP equation in [13] was developed underlying the bi-Hamiltonian structure $m_t = B_0 \frac{\delta H_{-1}}{\delta m}$.

DP equation investigated at $\kappa = 0$ can be also cast into the classical evolution equation $u_t = F(u, u_x, u_{xx}, u_{xxx}, \ldots)$, where $F = 3u_x u_{xx} + u u_{xxx} + u_{txx} - 4u u_x$. By definition, an evolution equation has its conservation laws provided that there exist a flux function Φ and a conserved density ρ which render the equation $\rho_t = \Phi_x$ [16]. In DP equation, $\rho = m(\equiv u - u_{xx})$ and $F = 2u^2 - \frac{3}{2}u_x^2 - \frac{1}{2}u_x^2 + u u_{xx}$ [17]. As a result, DP equation by definition has the conservation law given below

$$E_1(u) = \int u - u_{xx} dx. \tag{5}$$

For the other two density functions, which are $\rho = (u - u_{xx})(4 - \partial_x^2)^{-1} u$ and u^3, and their respective flux functions Φ, the equation $\rho_t = \Phi_x$ holds as well. As a result, two of the infinitely many conservation laws in DP equation are as follows

$$E_2(u) = \int (u - u_{xx})(4 - \partial_x^2)^{-1} u dx, \tag{6}$$

$$E_3(u) = \int u^3 dx. \tag{7}$$

These conservation laws in DP equation are much weaker than those in CH equation. Because of the existing Lax pair in (2) and (3) and the available bi-Hamiltonian structure in (4), DP equation is completely integrable [3].

Since CH and DP equations accommodate essentially different invariants and bi-Hamiltonian structures, the numerical methods capable of preserving these invariants are advantageous [13]. In the past, a great deal of effort has been made to preserve these distinguished conserved quantities within either the finite difference framework [18–20] or the Galerkin framework [21]. In this study we intend to develop an invariant-preserving finite difference scheme for the DP equation based on the symplectic scheme given in Section 4.1.

Like the CH equation, the currently investigated third-order equation is also amenable to multipeakon solution cast in an explicit form [22,23]. Unlike the CH equation, DP equation subject to an initially smooth solution supports shock solution [5]. Entropy weak solution is permitted when peakon collides with antipeakon. While a discontinuity can be formed in the non-dissipative DP equation, the conservation laws given in (5)–(7) remain valid all the time upon passing over the local discontinuity [6].

3. Solution algorithm of the DP equation

Besides the computationally challenging nonlinear term uu_x in the DP equation, there exist another two less numerically explored third-order derivative terms. They are known as the linear space–time dispersive term $-u_{xxt}$ and the nonlinear dispersive term $-uu_{xxx}$ that can spread out the localized wave. For getting a numerically more accurate balance of the wave steepening and spreading, a direct approximation of these third-order dispersion terms will be avoided. One trivial attempt is to reduce the differential order of the spatial derivative terms by introducing some auxiliary variables. The resulting reduction of the differential order helps to get a better prediction accuracy in a mesh having the same number of stencil points.

In the literature, two alternatives can be chosen to recast the DP scalar equation of a higher differential order form to its equivalent system of equations with the differential order being reduced by one. Two auxiliary momentum variables m and q_x^3, which are both equal to $u - u_{xx}$, can be defined to get their respective set of equations. In [16], the following set of equations is identical to the DP equation (1) at $\kappa = 0$

$$m = u - u_{xx}, \tag{8}$$

$$m_t + u m_x + 3u_x m = 0. \tag{9}$$

The other equivalent set of equations is as follows [24]

$$q_x^3 = u - u_{xx}, \tag{10}$$

$$q_t + uq_x = 0. \tag{11}$$

While the evolutionary equation (11) in the second set of DP equations is simpler than the convection–reaction equation (9) shown in the first set of equations, one normally adopts the $u - m$ formulation rather than the $u - q$ formulation mainly because of its resemblance to the $u - m$ formulation used more frequently in the calculation of CH equation.

The hyperbolic–elliptic equation (1) can be also splitted into the other set of equations, which includes two equations $u_t + uu_x = -P_x$ and $P - P_{xx} = 3\kappa^3 u + \frac{3}{2}u^2$, by introducing a Helmholtz operator for P [8]. This set of equations is referred to as the $u - P$ formulation. Because of the lack of solution smoothness and the possible formation of shock peakons for the case involving an initially smooth data, it is difficult to devise a good means to correctly compute the non-oscillatory values of u_x shown in the right-hand side of equation $u_t + uu_x = -P_x$. This motivated the modification of $u - P$ formulation by using a conservative variable to suppress numerical instability. At some locations where a peakon, at which u_x diverges, or even worse a shockpeakon, at which u has a jump (or discontinuity) appears, a physical flux term remains smooth. In this light, we will replace the term uu_x with the term $(u^2)_x$ shown in the $u - P$ formulation. In summary, the working set of equations chosen to avoid dealing with the computationally challenging terms u_{xxx}, u_{xxt}, and u_x (in case of a non-smooth solution) is as follows

$$u_t + \frac{1}{2}(u^2)_x = -P_x, \tag{12}$$

$$P - P_{xx} = 3\kappa^3 u + \frac{3}{2}u^2. \tag{13}$$

4. Discretization schemes

In the literature, much progress has been made on the theoretical study of DP equations. Most notably, the efforts have been devoted to prove well-posedness, explore blow-up and wave-breaking phenomena, demonstrate existence of the global weak solution, and derive exact traveling wave solution. Fewer numerical studies have been performed and this reason motivates the current numerical simulation of DP equation. While an apparent similarity exists between the CH and DP equations, Miyatake and Matsuo [13] pointed out that it is not proper to simply apply the comparatively well-developed CH schemes to solve the DP equation and vice versa [13]. The reason is that the invariants and their corresponding bi-Hamiltonian structures in CH equation are substantially different from those in DP equation. Our aim is to numerically reveal some of its salient mathematical features and the theoretical issues presented in Section 2.

For the approximation of the time-dependent differential equation (12), in this study the classical semi-discretization method is adopted. We will approximate the time derivative term before approximating the spatial derivative terms.

4.1. Symplectic time integration scheme for the time derivative term

Since Eq. (12) has a multi-symplectic structure, the time-stepping scheme cannot be chosen arbitrarily. To get a long-term accurate solution, a symplectic structure-preserving numerical integrator should be employed so as to properly conserve symplecticity in the currently investigated non-dissipative Hamiltonian system.

The sixth-order accurate symplectic Runge–Kutta scheme [25] is applied in this study for performing a long-time integration of the DP equation:

$$u^{(1)} = u^n + \Delta t\left[\frac{5}{36}F^{(1)} + \left(\frac{2}{9} + \frac{2\tilde{c}}{3}\right)F^{(2)} + \left(\frac{5}{36} + \frac{\tilde{c}}{3}\right)F^{(3)}\right], \tag{14}$$

$$u^{(2)} = u^n + \Delta t\left[\left(\frac{5}{36} - \frac{5\tilde{c}}{12}\right)F^{(1)} + \left(\frac{2}{9}\right)F^{(2)} + \left(\frac{5}{36} + \frac{5\tilde{c}}{12}\right)F^{(3)}\right], \tag{15}$$

$$u^{(3)} = u^n + \Delta t\left[\left(\frac{5}{36} - \frac{\tilde{c}}{3}\right)F^{(1)} + \left(\frac{2}{9} - \frac{2\tilde{c}}{3}\right)F^{(2)} + \frac{5}{36}F^{(3)}\right], \tag{16}$$

$$u^{n+1} = u^n + \Delta t\left[\frac{5}{18}F^{(1)} + \frac{4}{9}F^{(2)} + \frac{5}{18}F^{(3)}\right]. \tag{17}$$

where $\tilde{c} = \frac{1}{2}\sqrt{\frac{2}{5}}$ and $F^{(i)} = F(u^{(i)}, \overline{P}^{(i)}),\ i = 1, 2, 3$.

Based on the applied symplectic Runge–Kutta method, in order to calculate u^{n+1} from Eq. (17) we need to solve Eqs. (14)–(16) simultaneously (or implicitly) for obtaining the values of $u^{(1)},\ u^{(2)}$ and $u^{(3)}$. The Helmholtz equation (13) is then solved to get $\overline{P}^{(1)},\ \overline{P}^{(2)}$ and $\overline{P}^{(3)}$. Upon reaching the convergence criteria, we can get the solution u^{n+1} and then the solution $\overline{P}^{n+1}$. The

above iterative procedures will be repeated until the difference, cast in a L_2-norm form, of the solutions calculated from two consecutive iterations falls below the user's specified tolerance (10^{-9} in the current study).

4.2. Three-point seventh-order accurate upwinding combined compact difference scheme

To achieve the goal of accurately solving the equation over a longer simulation time, one can either employ a high-order finite-difference scheme or an optimized scheme [26]. In this study, the combined compact scheme presented in [27] is implemented in a smaller grid stencil for the approximation of derivative terms by considering the flux derivatives as the dependent variables at each grid point. Three derivative terms u_x, u_{xx} and u_{xxx} at each grid point are all - considered as the dependent variables so as to get a spectral-like resolution. We will describe below the proposed non-centered combined compact difference scheme in a stencil of three grid points when approximating the derivative terms $\frac{\partial u}{\partial x}$, $\frac{u^2 u}{\partial x^2}$ and $\frac{\partial^3 u}{\partial x^3}$

$$\left.\frac{\partial u}{\partial x}\right|_i + a_1 \left.\frac{\partial u}{\partial x}\right|_{i-1} + h\left(b_1 \left.\frac{\partial^2 u}{\partial x^2}\right|_{i-1} + b_2 \left.\frac{\partial^2 u}{\partial x^2}\right|_i + b_3 \left.\frac{\partial^2 u}{\partial x^2}\right|_{i+1}\right) + h^2\left(c_1 \left.\frac{\partial^3 u}{\partial x^3}\right|_{i-1} + c_3 \left.\frac{\partial^3 u}{\partial x^3}\right|_{i+1}\right) = \frac{1}{h}(d_1 u_{i-1} + d_2 u_i + d_3 u_{i+1}), \tag{18}$$

$$\left.\frac{\partial^2 u}{\partial x^2}\right|_i + \frac{1}{h}\left(-\frac{29}{16}\left.\frac{\partial u}{\partial x}\right|_{i-1} + \frac{29}{16}\left.\frac{\partial u}{\partial x}\right|_{i+1}\right) + \left(-\frac{5}{16}\left.\frac{\partial^2 u}{\partial x^2}\right|_{i-1} - \frac{5}{16}\left.\frac{\partial^2 u}{\partial x^2}\right|_{i+1}\right) + h\left(-\frac{1}{48}\left.\frac{\partial^3 u}{\partial x^3}\right|_{i-1} + \frac{1}{48}\left.\frac{\partial^3 u}{\partial x^3}\right|_{i+1}\right)$$
$$= \frac{1}{h^2}(4u_{i-1} - 8u_i + 4u_{i+1}), \tag{19}$$

$$\left.\frac{\partial^3 u}{\partial x^3}\right|_i + \frac{1}{h^2}\left(-\frac{105}{16}\left.\frac{\partial u}{\partial x}\right|_{i-1} - \frac{105}{16}\left.\frac{\partial u}{\partial x}\right|_{i+1}\right) + \frac{1}{h}\left(-\frac{15}{8}\left.\frac{\partial^2 u}{\partial x^2}\right|_{i-1} + \frac{15}{8}\left.\frac{\partial^2 u}{\partial x^2}\right|_{i+1}\right) + \left(-\frac{3}{16}\left.\frac{\partial^3 u}{\partial x^3}\right|_{i-1} - \frac{3}{16}\left.\frac{\partial^3 u}{\partial x^3}\right|_{i+1}\right)$$
$$= \frac{1}{h^3}\left(\frac{105}{16}u_{i-1} - \frac{105}{16}u_{i+1}\right). \tag{20}$$

Both of the second-order derivative term $\frac{\partial^2 u}{\partial x^2}$ and the third-order derivative term $\frac{\partial^3 u}{\partial x^3}$ are approximated using the center scheme. The coefficients shown in (18)–(20) can be determined simply by applying the Taylor series expansions for getting rid of the respective leading truncation error terms in their derived modified equations. The resulting orders of the formal accuracies become eighth and sixth, respectively [28].

For the description of the proposed upwinding compact difference scheme, only the case involving a positive-valued u will be described. The coefficients for the case involving a negative u value can be similarly derived. Determination of the eight weighting coefficients in (18) gets started by applying the Taylor series expansion for the terms u_{i-1}, u_{i+1}, $\left.\frac{\partial u}{\partial x}\right|_{i-1}$, $\left.\frac{\partial u}{\partial x}\right|_i$, $\left.\frac{\partial^2 u}{\partial x^2}\right|_{i-1}$, $\left.\frac{\partial^2 u}{\partial x^2}\right|_i$, $\left.\frac{\partial^2 u}{\partial x^2}\right|_{i+1}$, $\left.\frac{\partial^3 u}{\partial x^3}\right|_{i-1}$, and $\left.\frac{\partial^3 u}{\partial x^3}\right|_{i+1}$ with respect to u_i and then eliminating the leading error terms shown in the modified equation for $\frac{\partial u}{\partial x}$. For the wave-like term, the weighting coefficients in (18) determined solely by performing the truncation error analysis (or modified equation analysis) is insufficient to exhibit its characteristics. Besides the modified equation analysis applied to eliminate several leading discretization error terms, we need at the same time to perform Fourier analysis on (18) for the sake of getting the inherent wave-like characteristics.

The leading eight truncation error terms in the derived modified equation are eliminated first to get the following set of algebraic equations

$$d_1 + d_2 + d_3 = 0, \tag{21}$$

$$-a_1 - d_1 + d_3 = 1, \tag{22}$$

$$2a_1 + d_1 + d_3 - 2b_1 - 2b_2 - 2b_3 = 0, \tag{23}$$

$$d_1 - d_3 - 6b_1 + 6b_3 + 6c_1 + 6c_3 + 3a_1 = 0, \tag{24}$$

$$d_1 + d_3 - 12b_1 - 12b_3 + 24c_1 - 24c_3 + 4a_1 = 0, \tag{25}$$

$$d_1 - d_3 - 20b_1 + 20b_3 + 60c_1 + 60c_3 + 5a_1 = 0, \tag{26}$$

$$d_1 + d_3 - 30b_1 - 30b_3 + 120c_1 - 120c_3 + 6a_1 = 0, \tag{27}$$

$$d_1 - d_3 - 42b_1 + 42b_3 + 210c_1 + 210c_3 + 7a_1 = 0. \tag{28}$$

We are still short of one algebraic equation for uniquely determining all the nine introduced coefficients shown in (18) for u_x. For getting a better approximation of the first-order derivative term from Eq. (18), one should retain the dispersive nature embedded in $\frac{\partial u}{\partial x}$ as much as possible [29].

The expressions of the actual wavenumber for Eqs. (18)–(20) can be derived as

$$\begin{aligned}\mathbf{i}\beta h(a_1\exp(-\mathbf{i}\beta h)+1) \simeq{}& d_1\exp(-\mathbf{i}\beta h)+d_2+d_3\exp(\mathbf{i}\beta h)-(\mathbf{i}\beta h)^2(b_1\exp(-\mathbf{i}\beta h)+b_2+b_3\exp(\mathbf{i}\beta h))\\ &-(\mathbf{i}\beta h)^3(c_1\exp(-\mathbf{i}\beta h)+c_3\exp(\mathbf{i}\beta h)),\end{aligned} \tag{29}$$

$$\begin{aligned}\mathbf{i}\beta h\left(-\frac{29}{16}\exp(-\mathbf{i}\beta h)+\frac{29}{16}\exp(\mathbf{i}\beta h)\right) \simeq{}& 4\exp(-\mathbf{i}\beta h)-8+4\exp(\mathbf{i}\beta h)\\ &-(\mathbf{i}\beta h)^2\left(-\frac{5}{16}\exp(-\mathbf{i}\beta h)+1-\frac{5}{16}\exp(\mathbf{i}\beta h)\right)\\ &-(\mathbf{i}\beta h)^3\left(-\frac{1}{48}\exp(-\mathbf{i}\beta h)+\frac{1}{48}\exp(\mathbf{i}\beta h)\right),\end{aligned} \tag{30}$$

$$\begin{aligned}\mathbf{i}\beta h\left(-\frac{105}{16}\exp(-\mathbf{i}\beta h)-\frac{105}{16}\exp(\mathbf{i}\beta h)\right) \simeq{}& \frac{105}{16}\exp(-\mathbf{i}\beta h)-\frac{105}{16}\exp(\mathbf{i}\beta h)\\ &-(\mathbf{i}\beta h)^2\left(-\frac{15}{8}\exp(-\mathbf{i}\beta h)+\frac{15}{8}\exp(\mathbf{i}\beta h)\right)\\ &-(\mathbf{i}\beta h)^3\left(-\frac{3}{16}\exp(-\mathbf{i}\beta h)+1-\frac{3}{16}\exp(\mathbf{i}\beta h)\right).\end{aligned} \tag{31}$$

Our strategy of reducing dispersion error for the approximated first-order derivative term is to get an excellent match of the exact wavenumber with the numerical wavenumber. This amounts to equating the effective wavenumbers β, β'' and β''' to those shown in the right-hand sides of Eqs. (32)–(34) [29]. We can, as a result, express β, β'' and β''' as follows

$$\begin{aligned}\mathbf{i}\beta' h(a_1\exp(-\mathbf{i}\beta h)+1) = {}& d_1\exp(-\mathbf{i}\beta h)+d_2+d_3\exp(\mathbf{i}\beta h)-(\mathbf{i}\beta'' h)^2(b_1\exp(-\mathbf{i}\beta h)+b_2+b_3\exp(\mathbf{i}\beta h))\\ &-(\mathbf{i}\beta''' h)^3(c_1\exp(-\mathbf{i}\beta h)+c_3\exp(\mathbf{i}\beta h)),\end{aligned} \tag{32}$$

$$\begin{aligned}\mathbf{i}\beta' hB\left(-\frac{29}{16}\exp(-\mathbf{i}\beta h)+\frac{29}{16}\exp(\mathbf{i}\beta h)\right) = {}& 4\exp(-\mathbf{i}\beta h)-8+4\exp(\mathbf{i}\beta h)\\ &-(\mathbf{i}\beta'' h)^2\left(-\frac{5}{16}\exp(-\mathbf{i}\beta h)+1-\frac{5}{16}\exp(\mathbf{i}\beta h)\right)\\ &-(\mathbf{i}\beta''' h)^3\left(-\frac{1}{48}\exp(-\mathbf{i}\beta h)+\frac{1}{48}\exp(\mathbf{i}\beta h)\right),\end{aligned} \tag{33}$$

$$\begin{aligned}\mathbf{i}\beta' h\left(-\frac{105}{16}\exp(-\mathbf{i}\beta h)-\frac{105}{16}\exp(\mathbf{i}\beta h)\right) = {}& \frac{105}{16}\exp(-\mathbf{i}\beta h)-\frac{105}{16}\exp(\mathbf{i}\beta h)\\ &-(\mathbf{i}\beta'' h)^2\left(-\frac{15}{8}\exp(-\mathbf{i}\beta h)+\frac{15}{8}\exp(\mathbf{i}\beta h)\right)\\ &-(\mathbf{i}\beta''' h)^3\left(-\frac{3}{16}\exp(-\mathbf{i}\beta h)+1-\frac{3}{16}\exp(\mathbf{i}\beta h)\right).\end{aligned} \tag{34}$$

By solving Eqs. (32)–(34), the derived expression of $\beta' h$ can be written in a complex function form.

The above derived numerical modified (or scaled) wavenumber $\beta' h$ will be used in the analysis of numerical errors computed from the proposed combined compact finite difference scheme. The real and imaginary parts of the numerical modified wavenumber $\beta' h$ are responsible respectively for the dispersion error (phase error) and the dissipation error (amplitude error). To get a better dispersive accuracy for β', it is therefore demanded that βh be close to $\Re[\beta' h]$, where $\Re[\beta' h]$ denotes the real part of $\beta' h$. This means that the magnitude of the integrated error function $E(\beta)$ defined below should be a very small positive magnitude over the integration range $-\frac{\pi}{2}\leqslant\beta h\leqslant\frac{\pi}{2}$

$$E(\beta)=\int_{-\frac{\pi}{2}}^{\frac{\pi}{2}}[W(\beta h-\Re[\beta' h])]^2 d(\beta h). \tag{35}$$

The weighting function W in (35) is the denominator of $(\beta h-\Re[\beta' h])$ [30]. Inclusion of the function W makes $E(\beta)$ to be analytically integrable.

To make the error function defined in $-\frac{\pi}{2}\leqslant\beta h\leqslant\frac{\pi}{2}$ to be positive and minimal, the extreme condition $\frac{\partial E}{\partial d_1}=0$ is enforced to minimize the numerical wavenumber error. This constraint equation will be solved together with another eight previously derived algebraic equations by way of performing modified equation analysis to get a higher dissipation accuracy as well as an improved dispersion accuracy. The resulting nine introduced unknown coefficients can be uniquely determined as $a_1=1.1875$, $b_1=0.23643236$, $b_2=-0.27774699$, $b_3=-0.01356764$, $c_1=0.01894044$, $c_3=0.00189289$, $d_1=-2.33613227$,

$d_2 = 2.48476453$ and $d_3 = -0.14863227$. The above upwinding scheme developed in a stencil of three grid points $i-1$, i and $i+1$ for $\frac{\partial u}{\partial x}$ has the spatial accuracy order of seventh according to the following derived modified equation

$$\frac{\partial u}{\partial x} = \frac{\partial u}{\partial x}\bigg|_{exact} - 0.65175737 \times 10^{-5} h^7 \frac{\partial^8 u}{\partial x^6} + 0.81653294 \times 10^{-7} h^9 \frac{\partial^{10} u}{\partial x^{10}} + H.O.T. \tag{36}$$

When $u < 0$, the proposed non-centered combined compact difference scheme can be similarly derived below in a three-point grid stencil for the approximation of the derivative term $\frac{\partial u}{\partial x}$

$$\frac{\partial u}{\partial x}\bigg|_i + 1.1875 \frac{\partial u}{\partial x}\bigg|_{i+1} + h\left(0.01356764 \frac{\partial^2 u}{\partial x^2}\bigg|_{i-1} + 0.27774699 \frac{\partial^2 u}{\partial x^2}\bigg|_i - 0.23643236 \frac{\partial^2 u}{\partial x^2}\bigg|_{i+1}\right) + h^2\left(0.00189289 \frac{\partial^3 u}{\partial x^3}\bigg|_{i-1} + 0.01894044 \frac{\partial^3 u}{\partial x^3}\bigg|_{i+1}\right) = \frac{1}{h}(0.14863227 u_{i-1} - 2.48476453 u_i + 2.33613227 u_{i+1}). \tag{37}$$

4.3. Discretization of $(u^2)_x$ and P_x

It has been well known that it is proper to approximate the convective term shown in Eqs. (18) and (37) in conservative form for the sake of enhancing numerical stability. In this light we are aimed to conserve the convective flux term $f_x = (u^2)_x$ across a cell of length h by means of

$$\frac{\partial f}{\partial x}\bigg|_i = \frac{f_{i+\frac{1}{2}} - f_{i-\frac{1}{2}}}{h}. \tag{38}$$

Define first the values of f^- at the half nodal points $i \pm \frac{1}{2}$ as follows for $u \geqslant 0$

$$f^-_{i+\frac{1}{2}} = d_1^* f_i + d_2^* f_{i+1} - \left[a_1^* f_{i-\frac{1}{2}} + h\left(b_1^* \frac{\partial f}{\partial x}\bigg|_{i-\frac{1}{2}} + b_2^* \frac{\partial f}{\partial x}\bigg|_{i+\frac{1}{2}} + b_3^* \frac{\partial f}{\partial x}\bigg|_{i+\frac{3}{2}}\right) + h^2\left(c_1^* \frac{\partial f^2}{\partial^2 x}\bigg|_{i-\frac{1}{2}} + c_2^* \frac{\partial f^2}{\partial^2 x}\bigg|_{i+\frac{3}{2}}\right)\right] \tag{39}$$

and

$$f^-_{i-\frac{1}{2}} = d_1^* f_{i-1} + d_2^* f_i - \left[a_1^* f_{i-\frac{3}{2}} + h\left(b_1^* \frac{\partial f}{\partial x}\bigg|_{i-\frac{3}{2}} + b_2^* \frac{\partial f}{\partial x}\bigg|_{i-\frac{1}{2}} + b_3^* \frac{\partial f}{\partial x}\bigg|_{i+\frac{1}{2}}\right) + h^2\left(c_1^* \frac{\partial f}{\partial x}\bigg|_{i-\frac{3}{2}} + c_2^* \frac{\partial f}{\partial x}\bigg|_{i+\frac{1}{2}}\right)\right]. \tag{40}$$

The coefficients a_i^*, b_i^*, c_i^* and d_i^* are then derived by comparing the coefficients derived in Eq. (18) for $\frac{\partial f}{\partial x}\big|_i$. After a term-by-term comparison of the coefficients, we can get the coefficients shown in (39) and (40) as $a_1^* = 1.1875$, $b_1^* = 0.23643236$, $b_2^* = -0.27774699$, $b_3^* = -0.01356764$, $c_1^* = 0.01894044$, $c_2^* = 0.00189289$, $d_1^* = -2.33613227$ and $d_2^* = -0.14863227$.

When $u < 0$, the values of f^+ at the half nodal points $i \pm \frac{1}{2}$ are as follows

$$f^+_{i+\frac{1}{2}} = 0.14863227 f_i + 2.33613227 f_{i+1} - \left[1.1875 f_{i+\frac{3}{2}} + h\left(0.01356764 \frac{\partial f}{\partial x}\bigg|_{i-\frac{1}{2}} + 0.27774699 \frac{\partial f}{\partial x}\bigg|_{i+\frac{1}{2}} - 0.23643236 \frac{\partial f}{\partial x}\bigg|_{i+\frac{3}{2}}\right) + h^2\left(0.00189289 \frac{\partial f^2}{\partial^2 x}\bigg|_{i-\frac{1}{2}} + 0.01894044 \frac{\partial f^2}{\partial^2 x}\bigg|_{i+\frac{3}{2}}\right)\right] \tag{41}$$

and

$$f^+_{i-\frac{1}{2}} = 0.14863227 f_{i-1} + 2.33613227 f_i - \left[1.1875 f_{i+\frac{1}{2}} + h\left(0.01356764 \frac{\partial f}{\partial x}\bigg|_{i-\frac{3}{2}} + 0.27774699 \frac{\partial f}{\partial x}\bigg|_{i-\frac{1}{2}} - 0.23643236 \frac{\partial f}{\partial x}\bigg|_{i+\frac{1}{2}}\right) + h^2\left(0.00189289 \frac{\partial f^2}{\partial^2 x}\bigg|_{i-\frac{3}{2}} + 0.01894044 \frac{\partial f^2}{\partial^2 x}\bigg|_{i+\frac{1}{2}}\right)\right]. \tag{42}$$

Two flux terms $f_{i\pm\frac{1}{2}}$ shown in (38) are given below

$$f_{i+\frac{1}{2}} = \begin{cases} f^-_{i+\frac{1}{2}}; & \frac{f_{i+1}-f_i}{u_{i+1}-u_i} \geqslant 0, \\ f^+_{i+\frac{1}{2}}; & \frac{f_{i+1}-f_i}{u_{i+1}-u_i} < 0 \end{cases} \tag{43}$$

and

$$f_{i-\frac{1}{2}} = \begin{cases} f^-_{i-\frac{1}{2}}; & \frac{f_i-f_{i-1}}{u_i-u_{i-1}} \geqslant 0, \\ f^+_{i-\frac{1}{2}}; & \frac{f_i-f_{i-1}}{u_i-u_{i-1}} < 0. \end{cases} \tag{44}$$

To resolve the possible discontinuities predicted in the solution, the ULTIMATE conservative finite difference strategy presented in [31] is employed.

A central-type three-point combined compact difference (CCD) scheme [32] with the sixth-order accuracy is used to approximate the gradient term P_x shown in (12) as follows

$$\frac{7}{16}\frac{\partial P}{\partial x}\Big|_{i-1}+\frac{\partial P}{\partial x}\Big|_{i}+\frac{7}{16}\frac{\partial P}{\partial x}\Big|_{i+1}=\frac{15}{16h}(-P_{i-1}+P_{i+1})-\left(\frac{h}{16}\frac{\partial^2 P}{\partial x^2}\Big|_{i-1}-\frac{h}{16}\frac{\partial^2 P}{\partial x^2}|_{i+1}\right), \tag{45}$$

$$-\frac{1}{8}\frac{\partial^2 P}{\partial x^2}\Big|_{i-1}+\frac{\partial^2 P}{\partial x^2}\Big|_{i}-\frac{1}{8}\frac{\partial^2 P}{\partial x^2}\Big|_{i+1}=\frac{1}{h^2}(3P_{i-1}-6P_i+3P_{i+1})-\frac{1}{h}\left(-\frac{9}{8}\frac{\partial P}{\partial x}\Big|_{i-1}+\frac{9}{8}\frac{\partial P}{\partial x}\Big|_{i+1}\right). \tag{46}$$

The above CCD scheme developed in the stencil of three grid points $i-1$, i and $i+1$ for $\frac{\partial P}{\partial x}$ is sixth-order accurate.

4.4. Three-point sixth-order accurate compact Helmholtz scheme

To get a more accurate solution P from the inhomogeneous Helmholtz equation (13), one can always introduce more grid points in the domain of interest. While the prediction accuracy can be easily improved in this way, the computational cost becomes considerable because of the required matrix calculation. For developing an efficient and accurate numerical scheme, the following sixth-order accurate compact difference scheme is proposed in a three-point stencil.

The prototype inhomogeneous equation with $G(\equiv 3\kappa^3 u+\frac{3}{2}u^2)$given below will be considered

$$\frac{\partial^2 P}{\partial x^2}-kP=G(x). \tag{47}$$

The values of $\frac{\partial^2 P}{\partial x^2}$, $\frac{\partial^4 P}{\partial x^4}$ and $\frac{\partial^6 P}{\partial x^6}$ at an interior point i are denoted as $\frac{\partial^2 P}{\partial x^2}|_i=s_i$, $\frac{\partial^4 P}{\partial x^4}|_i=v_i$, $\frac{\partial^6 P}{\partial x^6}|_i=w_i$. Development of the compact finite difference equation for (47) at the node i starts with relating the derivative terms v, s and w with P by means of the equation given below

$$\delta_0 h^6 w_i+\gamma_0 h^4 v_i+\beta_0 h^2 s_i=\alpha_1 P_{i+1}+\alpha_0 P_i+\alpha_{-1}P_{i-1}. \tag{48}$$

The elliptic nature of the Eq. (47) motivates us to set $\alpha_1=\alpha_{-1}$. By expanding the terms $P_{i\pm1}$ with respect to P_i in Taylor series and then substituting these two expansion equations into Eq. (48), we have

$$\delta_0 h^6 w_i+\gamma_0 h^4 v_i+\beta_0 h^2 s_i=(\alpha_0+2\alpha_1)P_i+2\alpha_1\left[\frac{h^2}{2!}\frac{\partial^2 P_i}{\partial x^2}+\frac{h^4}{4!}\frac{\partial^4 P_i}{\partial x^4}+\frac{h^6}{6!}\frac{\partial^6 P_i}{\partial x^6}+\frac{h^8}{8!}\frac{\partial^8 P_i}{\partial x^8}+\cdots\right]. \tag{49}$$

Through a term-by-term comparison of the derivative terms shown in Eq. (49), a set of five algebraic equations can be derived. Hence, the introduced free parameters are determined as $\alpha_1=\alpha_{-1}=-1$, $\alpha_0=2$, $\beta_0=-1$, $\gamma_0=-\frac{1}{12}$ and $\delta_0=-\frac{1}{360}$. Since $w_i=k^3P_i+k^2G_i+k\frac{\partial^2 G_i}{\partial x^2}+\frac{\partial^4 G_i}{\partial x^4}$, $v_i=k^2P_i+kG_i+\frac{\partial^2 G_i}{\partial x^2}$ and $s_i=kP_i+G_i$, Eq. (48) can then be further expressed as

$$P_{i+1}-\left(2+h^2k+\frac{1}{12}h^4k^2+\frac{1}{360}h^6k^3\right)P_i+P_{i-1}=h^2G_i+\frac{1}{12}h^4\left(kG_i+\frac{\partial^2 G_i}{\partial x^2}\right)+\frac{1}{360}h^6\left(k^2G_i+k\frac{\partial^2 G_i}{\partial x^2}+\frac{\partial^4 G_i}{\partial x^4}\right). \tag{50}$$

The corresponding modified equation for (47) shown below confirms that the current three-point compact difference scheme is indeed sixth-order accurate

$$\frac{\partial^2 P}{\partial x^2}-kP=G+\frac{h^6}{20160}\frac{\partial^8 P}{\partial x^8}+\frac{h^8}{1814400}\frac{\partial^{10}P}{\partial x^{10}}+\cdots+H.O.T. \tag{51}$$

The V-cycle multigrid method is implemented in this study by using the fully-weighted projection/ prolongation operators. The red–black Gauss–Seidel smoother is employed to solve the system of algebraic equations using the proposed scheme.

4.5. Final solution algorithm

For the sake of clearness, the procedures of getting the solution u^{n+1} from u^n using the proposed solution algorithm are summarized as follows:

Step 1 : Start from the initial guess for $u^{(i)}$, denoted as $u^{[0],(i)}$ for $i=1,2,3$, which is set at u^n.
Step 2 : The Helmholtz equation (13) is solved to get $P^{[0],(i)}$ for $i=1,2,3$ by the proposed three-point sixth-order accurate compact Helmholtz scheme described in Section 4.2.
Step 3 : Discretize $f_x^{[0],(i)}$ and $P_x^{[0],(i)}$ by the scheme given in Section 4.3 so as to get $F^{[0],(i)}$, $i=1,2,3$.
Step 4 : Based on the applied symplectic Runge–Kutta method presented in Section 4.1 for (12), Eqs. (14),(15),(16) are solved simultaneously (or implicitly) for getting the values of $u^{[1],(i)}$, $i=1,2,3$.

Table 1
The predicted L_2-error norms at $t = 1$ for the calculations obtained in $-40 \leqslant x \leqslant 6$ and at $\Delta t = 0.0005$ using three different mesh sizes. This problem is described in Section 4.2.

Grid number	L_2 error norms	Rates of convergence
64	7.99681E−3	
512	1.95223E−7	5.10734
1024	1.82633E−9	6.74003

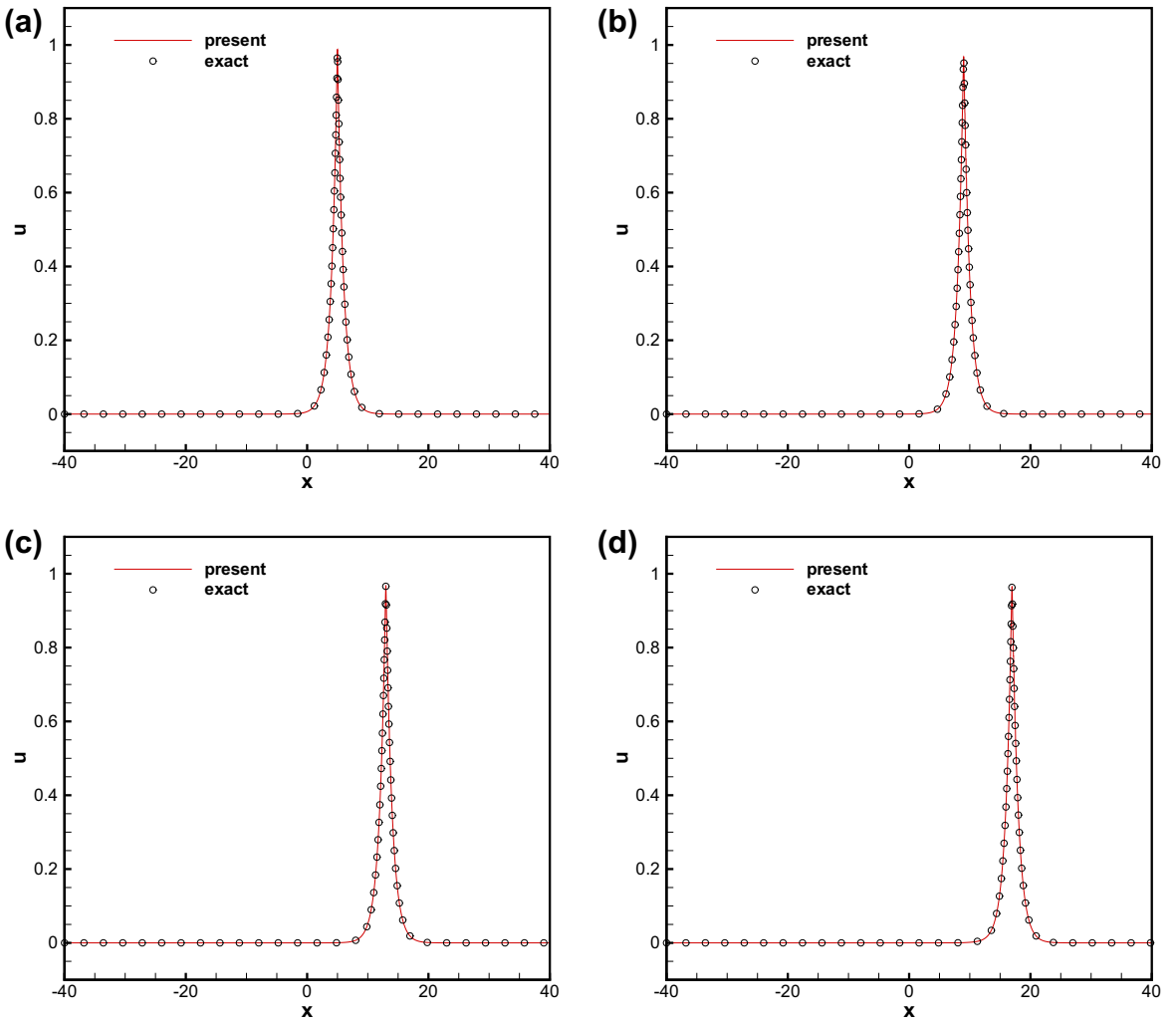

Fig. 1. Comparison of the predicted and exact peakon solutions [6] computed in 2048 grids at different times. (a) $t = 5.0$; (b) $t = 9.0$; (c) $t = 13.0$; (d) $t = 17.0$.

Step 5 : Repeat the calculation from Step2 to Step4 until the residuals, cast in the maximum norms, of Eqs. (14),(15),(16) satisfy the convergence criterion $\mathbf{Max}_{x_{j,j=1,N}} |u^{[\bar{k}+1],(i)} - u^{[\bar{k}],(i)}| \leqslant 10^{-9}$**, where** N **denotes the number of grid points and** $\bar{k}$ **is the** k**-th iteration number.**

Step 6 : Use Eq. (17) to update u^{n+1}**.**

5. Numerical results

The problems under current investigation include the simulations of a single peakon, peakon–peakon, peakon–antipeakon, shock peakon, and peakon–antipeakon–shockpeakon triple interaction. Periodic boundary condition is prescribed at two ends for all the test problems investigated at $\kappa = 0$.

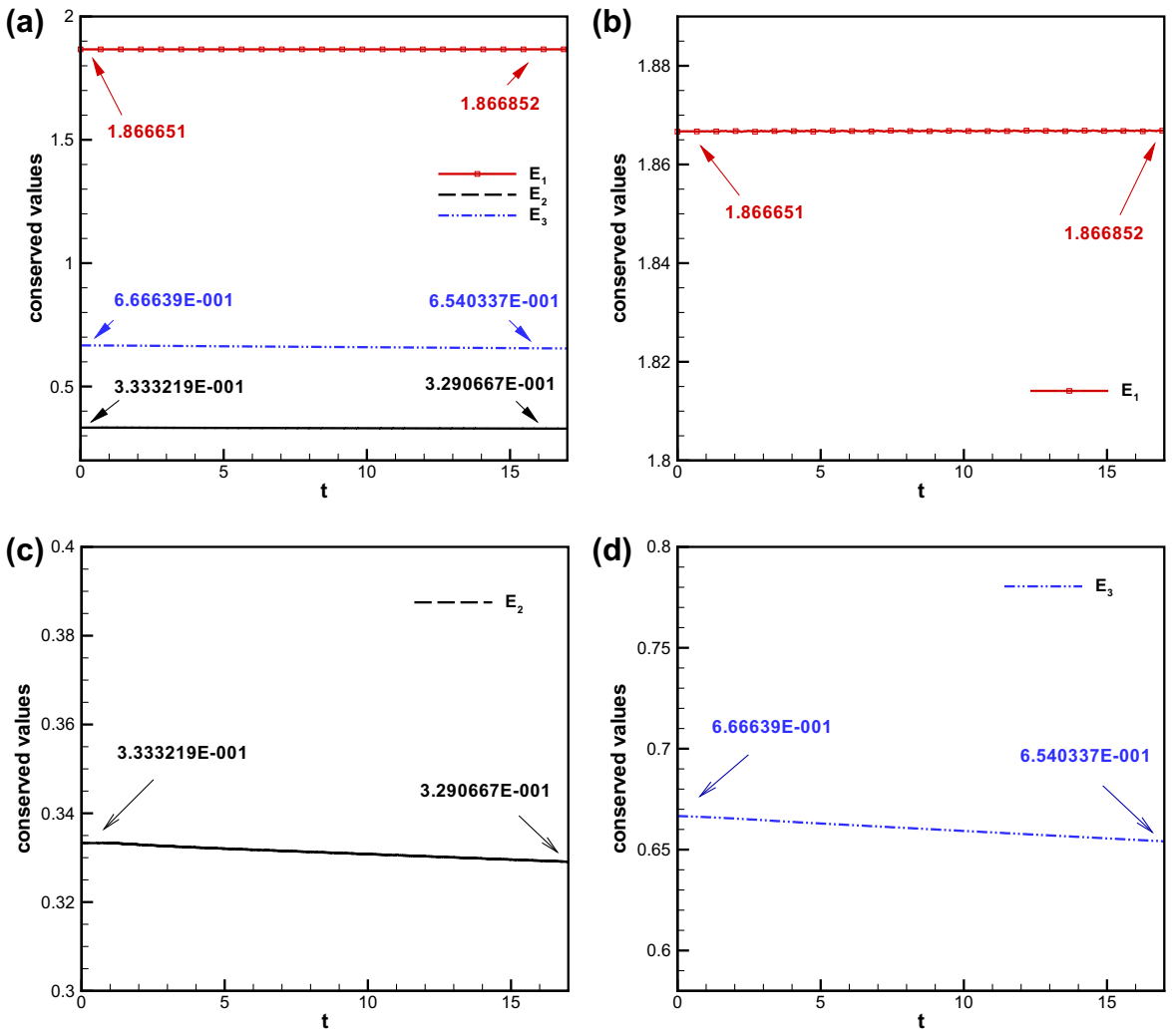

Fig. 2. (a) Plot of the computed values E_1, E_2 and E_3 against time for the investigated peakon problem in 2048 grids; (b) The Hamiltonian is enlarged from (a) for E_1; (c) The Hamiltonian is enlarged from (a) for E_2; (d) The Hamiltonian is enlarged from (a) for E_3.

5.1. Single peakon travelling solution

A delicate balance between the nonlinear and dispersive effects in DP equation leads to a confined solitary traveling wave solution $u(x,t) = ce^{-|x-ct|}$. This type of traveling wave solution exists even in the absence of linear dispersion term (or $\kappa = 0$ in Eq. (1)). In the above traveling wave solution, c denotes the constant wave speed. It is worthy to note that the completely integrable KdV, CH and the currently investigated DP equations possess solitons as the traveling wave solutions. Note also that this traveling wave solution is smooth everywhere except at the wave crest. We call, as a result, such a solution as a peakon (peaked soliton).

A single peakon propagated at $c = 1$ will be predicted in the domain [-40, 40] with the total number of 2048 uniformly distributed grid points. To begin with, the applied method is validated in view of the predicted L_2-error norms and the spatial rates of convergence shown in Table 1.

The waveforms predicted at $t = 5$, $t = 9$, $t = 13$ and $t = 17$ are plotted together with the exact solution. We can see clearly from Fig. 1 that the moving peakon is well resolved without generating any numerical oscillation. In addition, the conserved laws given in (5)–(7) are numerically confirmed, thereby giving an indirect validation of the proposed symplectic scheme for solving the non-dissipative DP equation. In Fig. 2, all the values of E_1, E_2 and E_3 are decreased by negligibly small amounts.

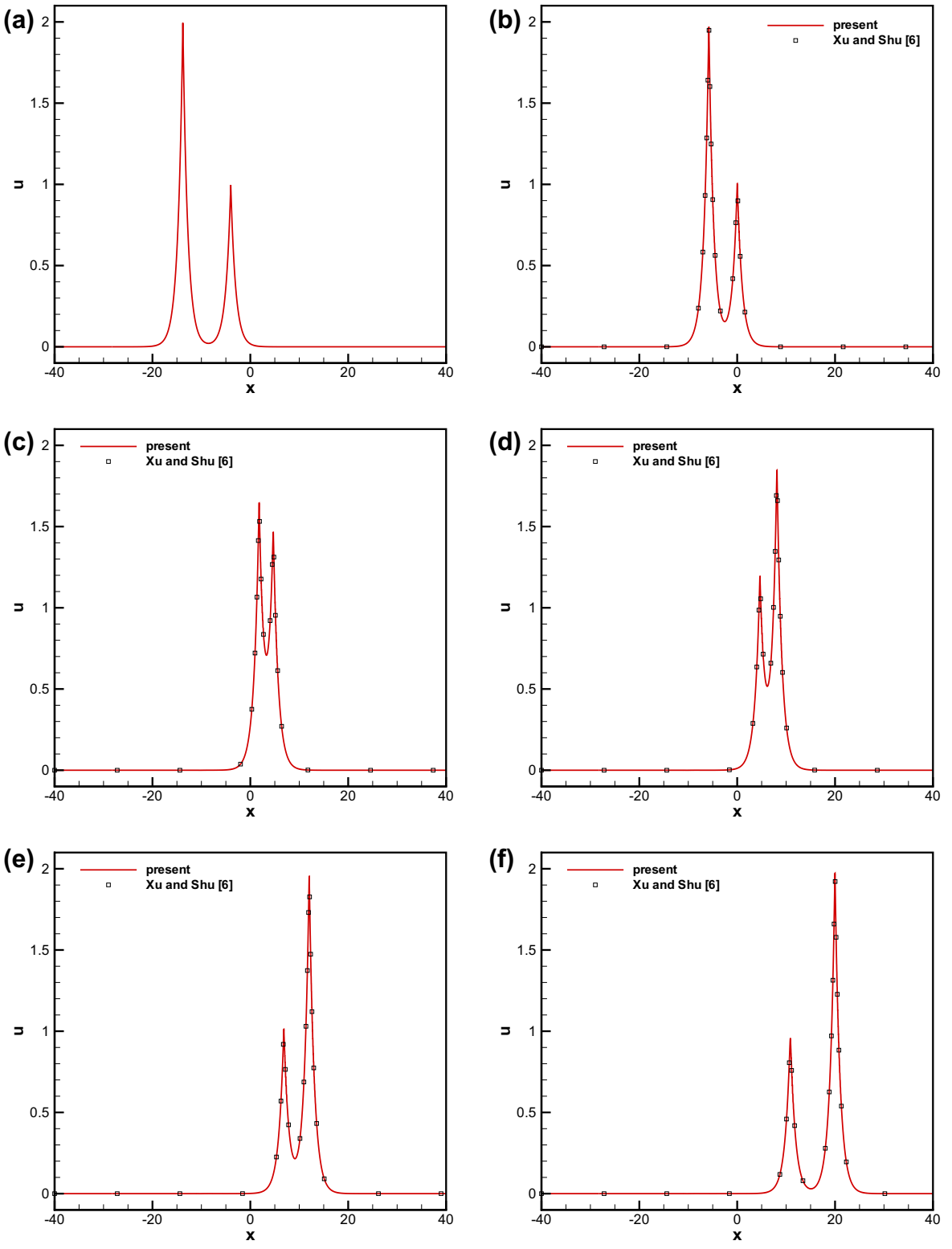

Fig. 3. Comparison of the predicted and numerical peakon–peakon solutions computed in 2048 grids at different times. (a) $t = 0.0$; (b) $t = 4.0$; (c) $t = 8.0$; (d) $t = 10.0$; (e) $t = 12.0$; (f) $t = 16.0$.

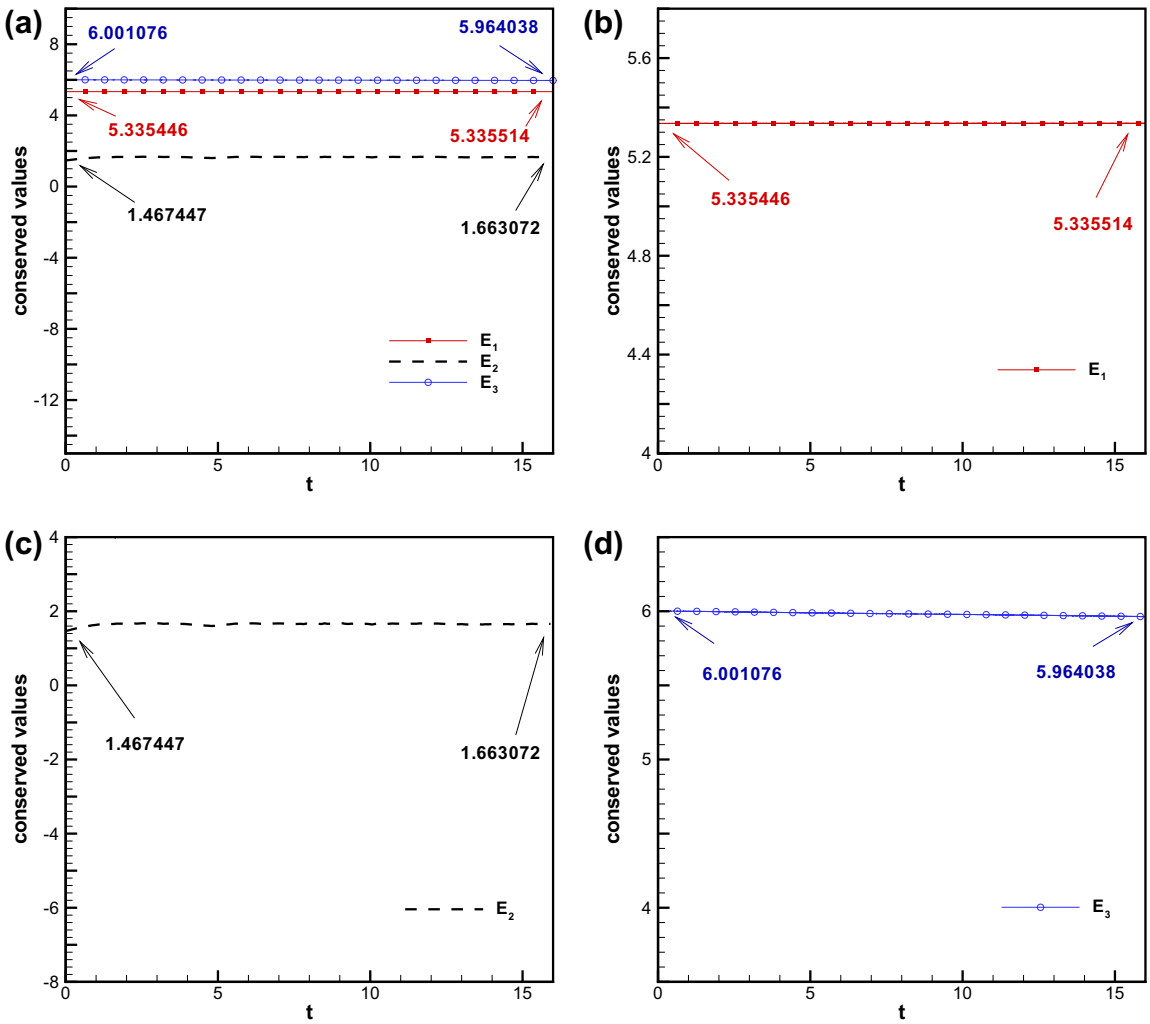

Fig. 4. (a) Plot of the computed values E_1, E_2 and E_3 against time for the investigated peakon–peakon interaction problem in 2048 grids; (b) The Hamiltonian is enlarged from (a) for E_1; (c) The Hamiltonian is enlarged from (a) for E_2; (d) The Hamiltonian is enlarged from (a) for E_3.

5.2. Peakon–peakon interaction

Soliton (or solitary wave) by definition can asymptotically preserve its shape and velocity upon encountering a nonlinear interaction with other solitary waves. In DP equation, we will numerically reveal that one peakon can interact with the other peakon through an elastic process.

Two peakons propagating along the same direction will be investigated subject to the following initial data [5,6,8] in a domain of $-40 \leqslant x \leqslant 40$

$$u(x, t = 0) = c_1 e^{-|x-x_1|} + c_2 e^{-|x-x_2|}. \tag{52}$$

These two investigated peakons move rightwards at the speeds of $c_1 = 2$ and $c_2 = 1$. At $\kappa = 0$, the Degasperis–Procesi equation will be solved at $x_1 = -13.792$ and $x_2 = -4$. In Fig. 3, we can see that the time-evolving two-peakon solutions predicted in a domain of 2048 uniformly discretized grids compare excellently with the numerical results given in [6]. In addition to the predicted oscillation-free solutions, the Hamiltonians plotted in Fig. 4 confirm that the proposed scheme is applicable to simulate the transport phenomenon of a moving pair of peakon–peakon waves.

5.3. Peakon–antipeakon interaction problem

DP equation admits peakons as well as shock peakons. Peakon solution normally has jumps in u_x but not in the solution u itself. Shockpeakon forms naturally in the DP equation in case of a peakon–antipeakon collision. In CH equation, peakon and

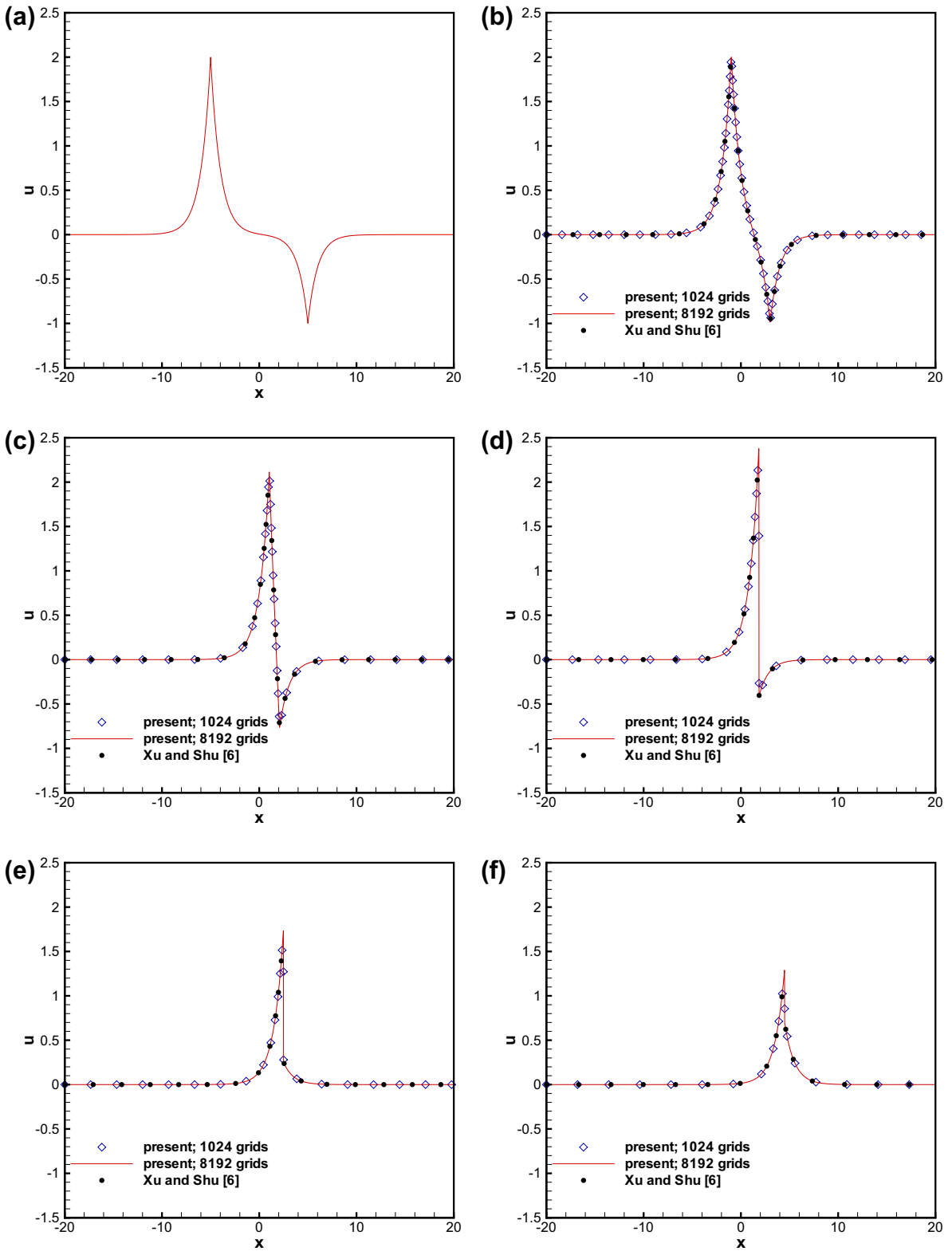

Fig. 5. Comparison of the predicted and numerical peakon–antipeakon solutions computed in 1024 and 8192 grids at different times. (a) $t = 0.0$; (b) $t = 2.0$; (c) $t = 3.0$; (d) $t = 3.3626$; (e) $t = 4.0$; (f) $t = 6.0$.

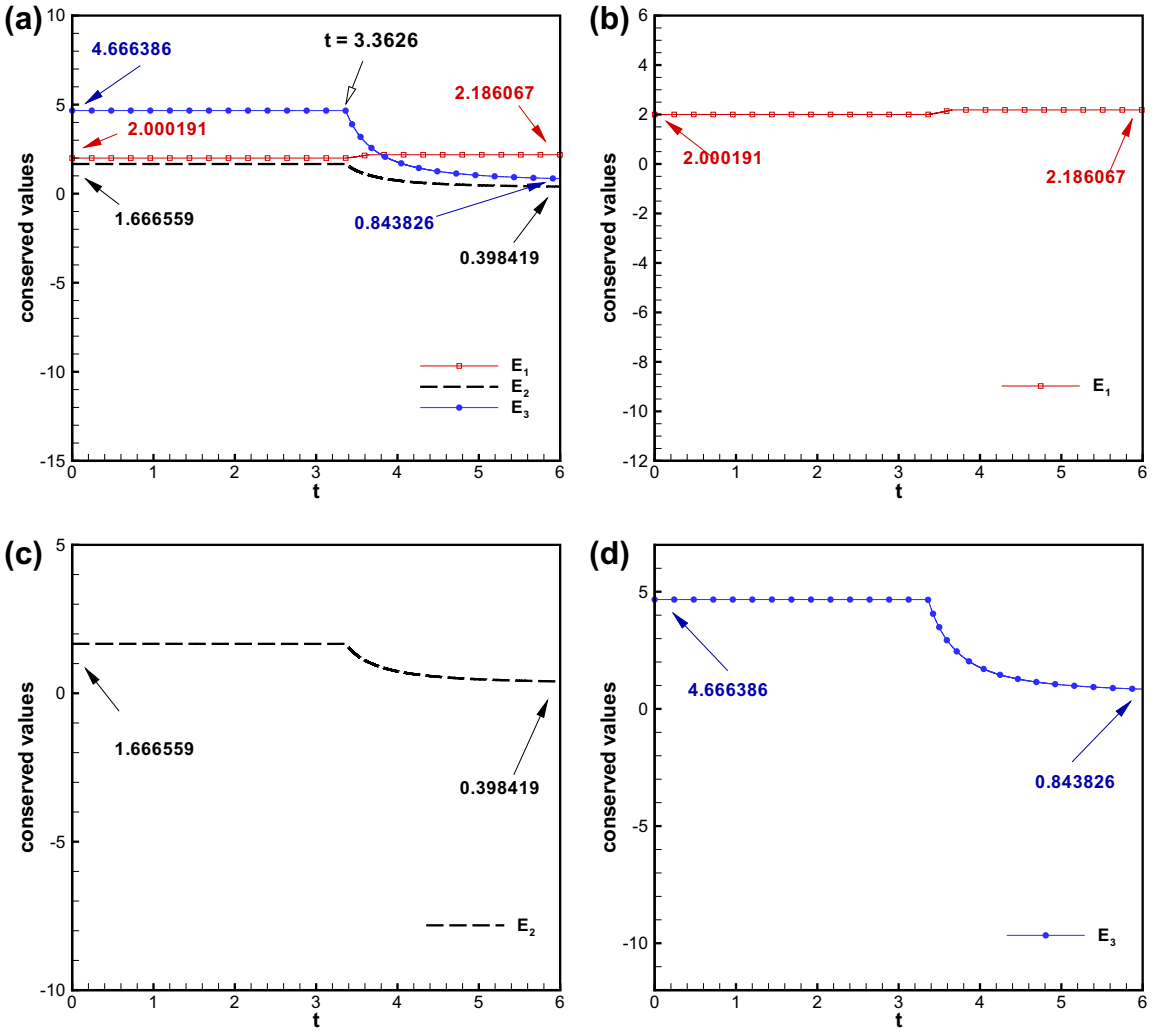

Fig. 6. (a) Plot of the computed values E_1, E_2 and E_3 against time for the investigated peakon–antipeakon interaction problem in 2048 grids; (b) The Hamiltonian is enlarged from (a) for E_1; (c) The Hamiltonian is enlarged from (a) for E_2; (d) The Hamiltonian is enlarged from (a) for E_3.

antipeakon pass through each other after the peakon–antipeakon collision. DP solution develops, however, a jump discontinuity in u. The presence of shockpeakon solution means that DP equation admits solution that is less regular than the CH equation. This novel peakon–antipeakon interaction feature, which makes in fact a dramatic difference between the DP and CH equations, will be numerically demonstrated in this study.

The interaction of peakon $c_1 e^{-|x-x_1|}$ $(c_1 > 0)$ and antipeakon $c_2 e^{-|x-x_2|}$ $(c_2 < 0)$ will be numerically investigated. This peakon–antipeakon interaction problem is solved in the domain $-20 \leqslant x \leqslant 20$ with the initial condition given by [5,6,8]

$$u(x, t = 0) = c_1 e^{-|x-x_1|} + c_2 e^{-|x-x_2|}. \tag{53}$$

In the above, we specify $c_1 = 2$, $c_2 = -1$, $x_1 = 2$, and $x_2 = -1$. The numbers of cells used in this simulation study are 1024 and 8192.

Fig. 5 shows the comparison of the solution computed from the proposed scheme and the solution given in [6]. In this calculation, the ULTIMATE conservative finite difference limiter given in [31] in adopted to suppress oscillations possibly occurring near the discontinuity when the shockpeakon is formed. We can see clearly from Fig. 5 that no oscillation has been found during the peakon and anti-peakon interaction. After the collision at the time $t = 3.3626$, the solution of DP equation is found to develop into a discontinuity in u, known as the shockpeakon. Note that no shockpeakon can arise from the CH equation is case of the peakon–antipeakon collision. Fig. 6 shows that all the computed Hamiltonians defined in (5)–(7) remain unchanged prior to the collision time at $t = 3.3626$. After the time at $t = 3.3626$, when peakon collides with the antipeakon, the Hamiltonian E_1 remains unchanged but the Hamiltonians E_2 and E_3, which contain u, of the DP equation shown in Fig. 6 are no longer preserved. This computational finding has been pointed out perviously by Lundmark without giving a

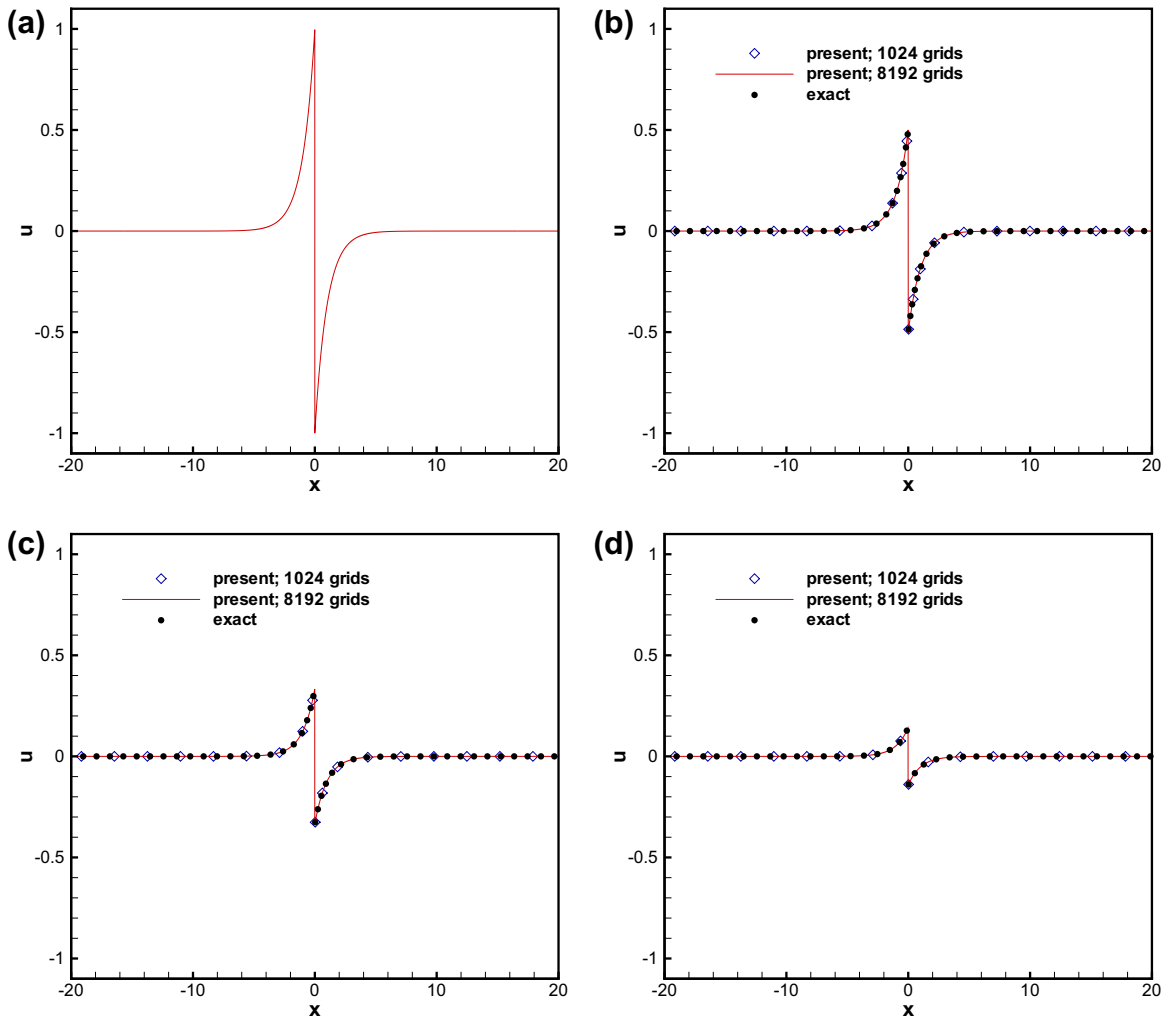

Fig. 7. Comparison of the predicted and exact shock peakon solutions computed in 1024 and 8192 grids at different times. (a) $t = 0.0$; (b) $t = 1.0$; (e) $t = 2.0$; (d) $t = 6.0$.

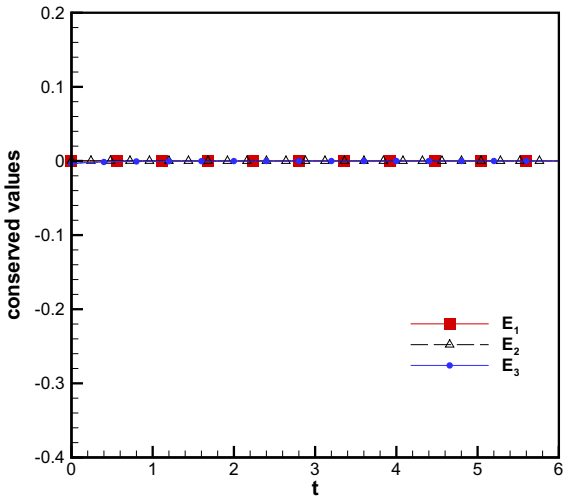

Fig. 8. Plot of the computed values E_1, E_2 and E_3 against time for the investigated shock peakon problem in 8192 grids.

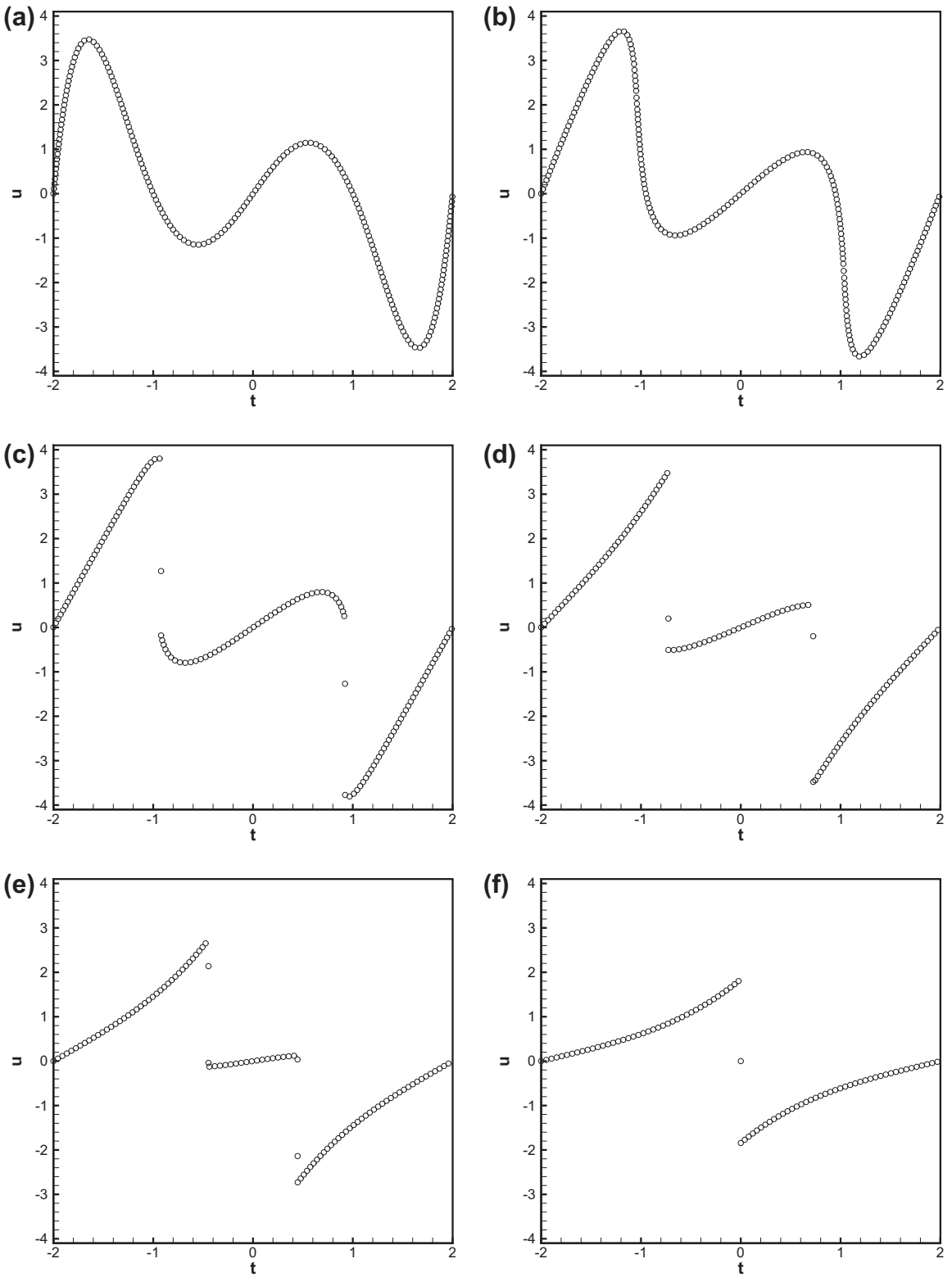

Fig. 9. The predicted shock-formation solutions in a domain of 4096 grids at different times. (a) $t = 0.1$; (b) $t = 0.12$; (c) $t = 0.18$; (d) $t = 0.3$; (e) $t = 0.5$; (f) $t = 0.9$.

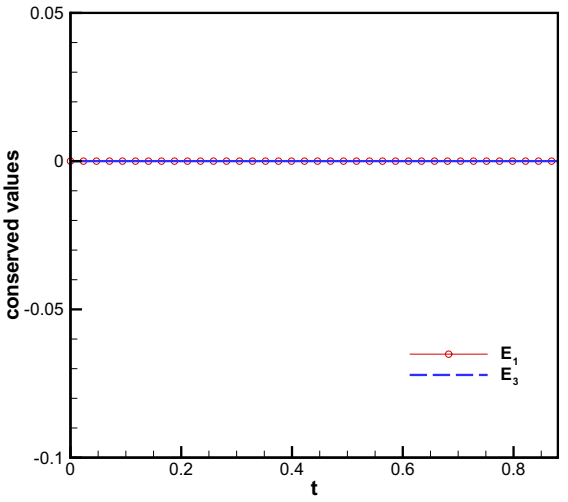

Fig. 10. Plot of the computed values E_1 and E_3 against time for the investigated shock formation problem in 4096 grids.

computational evidence [5]. Whether or not the DP equation can truly remain non-dissipative in case of peakon–antipeakon collision is still an open question [13].

5.4. Shock peakon solution

In this example, the analytic problem regarding the evolution of the shockpeakon given below will be studied numerically in $[-30, 30]$ [6]

$$u(x,t) = -\frac{1}{t+1} sign(x) e^{-|x|}. \tag{54}$$

The shockpeakon profiles are shown in Fig. 7 at different times. In this study, the simulations carried out in 1024 and 8192 grids are aimed to resolve shock peakon. We can see clearly that shockpeakon profiles are both well resolved without showing numerical oscillations. As before, three Hamiltonians are calculated and plotted in Fig. 8 to show the ability of employing the proposed scheme to conserve Hamiltonians even for the case involving a shock solution.

5.5. Shock formation

An example with the initial condition given below is also studied

$$u(x, t=0) = e^{0.5x^2} sin(\pi x). \tag{55}$$

The time-evolving shock formation was predicted in a domain of 4096 uniformly discretized grids. Fig. 9 shows the computed solution that was seen to agree with the numerical results presented in [7,6,8] up to $t = 0.9$. Only a single transition point is predicted to appear at the position of shock and no numerical oscillation has been observed. As before, the Hamiltonians E_1 and E_3 plotted in Fig. 10 show good discrete conservation against time for the investigated non-dissipative DP equation.

5.6. Peakon–antipeakon–shockpeakon interaction

The interaction among a pair of symmetric peakon–antipeakon and one stationary shock peakon was studied theoretically by Lundmark in [5] and numerically by the authors in [7,6,8]. The initial condition for this peakon–antipeakon–shockpeakon problem is as follows

$$u(x, t=0) = e^{-|x+5|} + sign(x) e^{-|x|} - e^{-|x-5|}. \tag{56}$$

A total number of 16,384 grids is used in this study to resolve the peakon–antipeakon–shockpeakon interaction details in the domain $[-25, 25]$. In Fig. 11, we can see clearly that the complex wave interaction has been resolved quite well. Good conservation of the Hamiltonians E_1 and E_3 can be also seen as before in Fig. 12.

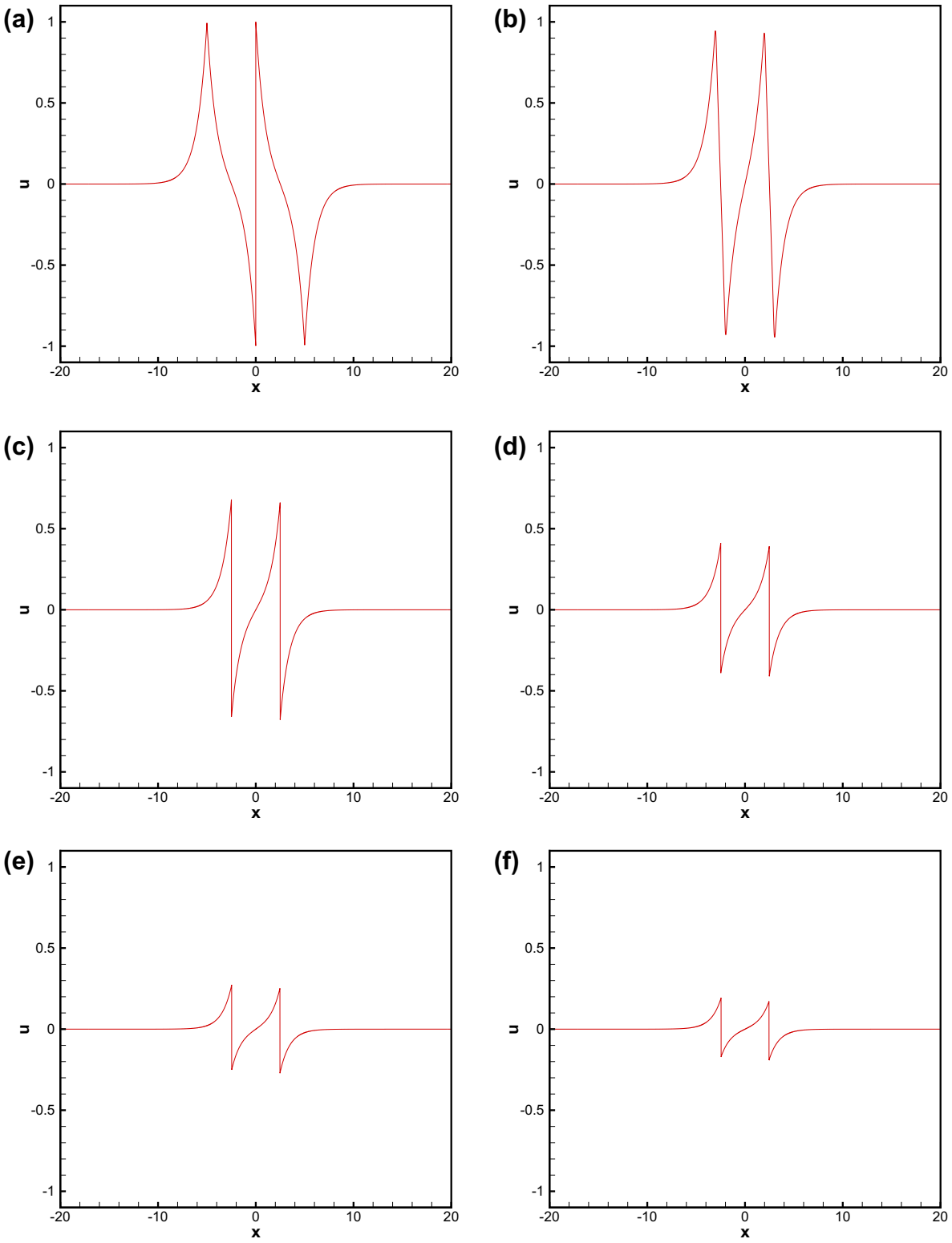

Fig. 11. The predicted peakon–antipeakon–shockpeakon interaction solutions in a domain of 16,384 grids at different times. (a) $t = 0.0$; (b) $t = 2.0$; (c) $t = 3.0$; (d) $t = 4.0$; (e) $t = 5.32$; (f) $t = 6.0$.

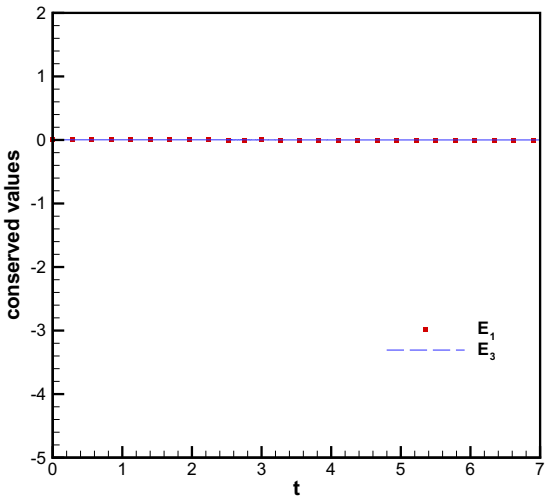

Fig. 12. Plot of the computed values E_1 and E_3 against time for the investigated peakon–antipeakon–shockpeakon interaction problem in 16,384 grids.

6. Concluding remarks

To reduce the differential order, the Degasperis–Procesi equation is recast to its equivalent conservative form. In the current $u - P$ formulation, the space–time mixed derivative term in the DP equation is eliminated and this elimination simplifies our computation. The time derivative term is approximated by the sixth-order accurate implicit symplectic Runge–Kutta scheme so that the scheme is unconditionally stable and the conserved properties in the non-dissipative DP equation can be numerically retained. As for the approximation of the first-order spatial derivative terms shown in the equation, a seventh-order accurate upwinding combined compact difference scheme is developed to minimize the numerical dispersion error. For the single peakon problem, the Hamiltonians in DP equation can be perfectly conserved all the time. For the peakon–peakon interaction problem, our simulation results clearly exhibit that peakons are interacted with each other elastically. For the peakon–antipeakon problem, a jump discontinuity known as the shockpeakon arises and it has been well resolved numerically at the time upon collision. All the Hamiltonians remain, however, unchanged before the time of collision. The DP equation, which permits a globally non-dissipative solution, is therefore numerically demonstrated before the time of collision. After the collision, only the Hamiltonians involving the solution itself are dissipative.

Acknowledgement

This research study is supported by National Science Council through the Grants NSC 98-2628-M-002-006 and 99-2221-E-002-225-MY3.

References

[1] T.B. Benjamin, J.L. Bona, J.J. Mahony, Model equations for long waves in nonlinear dispersive systems, Philos. Trans. R. Soc. Lond. Ser. A 272 (1972) 47–78.
[2] R. Camassa, D.D. Holm, An integrable shallow water equation with peaked solitons, Phys. Rev. Lett. 71 (1993) 1661–1664.
[3] A. Degasperis, D.D. Holm, A. Hone, A new integrable equation with peakon solutions, Theoret. Math. Phys. 133 (2002) 1463–1474.
[4] G.M. Coclite, K.H. Karlsen, On the well-posedness of the Degasperis–Procesi equation, J. Funct. Anal. 233 (2006) 60–91.
[5] H. Lundmark, Formation and dynamics of shock waves in the Degasperis–Procesi equation, J. Nonlinear Sci. 17 (2007) 169–198.
[6] Y. Xu, C.W. Shu, Local discontinuous Galerkin methods for the Degasperis–Procesi equation, Commun. Comput. Phys. 10 (2011) 474–508.
[7] G.M. Coclite, K.H. Karlsen, N.H. Risebro, Numerical schemes for computing discontinuous solutions of the Degasperis–Procesi equation, IMA J. Numer. Anal. 28 (1) (2008) 80–105.
[8] B.F.- Feng, Y. Liu, An operator splitting method for the Degasperis–Procesi equation, J. Comput. Phys. 228 (2009) 7805–7820.
[9] H.A. Hoel, A numerical scheme using multi-shockpeakons to compute solutions of the Degasperis–Procesi equation, Electron. J. Differ. Equ. 2007 (100) (2007) 1–22.
[10] J. Yan, C.W. Shu, A local discontinuous Galerkin method for KdV type equations, SIAM J. Numer. Anal. 40 (2002) 769–791.
[11] Y. Xu, C.W. Shu, A local discontinuous Galerkin method for the Camassa–Holm equation, SIAM J. Numer. Anal. 46 (2008) 1998–2021.
[12] Y. Xu, C.W. Shu, Local discontinuous Galerkin methods for high-order time-dependent partial differential equations, Commun. Comput. Phys. 7 (2010) 1–46.
[13] Y. Miyatake, T. Matsuo, Conservative finite difference schemes for the Degasperis–Procesi equation, J. Comput. Appl. Math. 236 (15) (2012) 3728–3740.
[14] Y. Zhou, Blow-up phenomenon for the integrable Degasperis–Procesi equation, Phys. Lett. A 328 (2004) 157–162.
[15] A.N.W. Hone, J.P. Wang, Propagation algebras and Hamiltonian operators for peakon equations, Inverse Prob. 19 (2003) 129–145.
[16] A. Degasperis, M. Procesi, Asymptotic integrability, in: A. Degasperis, G. Gaeta (Eds.), Symmetry and Perturbation Theory, World Scientific, Singapore, 1999, pp. 23–37.
[17] S. Saha, A Study on the *b* Family of Shallow Water Wave Equations, PhD Thesis, The University of Texas at Arlington, USA, Dec. 2008.

[18] D. Furihara, D. Mori, General derivation of finite difference schemes by means of a discrete variation, Trans. Jpn Soc. Ind. Appl. Math. 8 (1998) 317–340.
[19] E. Celledoni, V. Grimm, R.I. McLachlan, D.I. McLaren, D. O'Neale, B. Owren, G.R.W. Quispel, Preserving energy resp. dissipation in numerical PDEs, using the average vector field method, J. Comput. Phys. 231 (2012) 6770–6789.
[20] R.I. McLachlan, G.R.W. Quispel, N. Robidoux, Geometric integration using discrete gradients, Philos. Trans. R. Soc. Lond. A Math. Phys. Eng. Sci. 357 (1999) 1021–1045.
[21] T. Matsuo, Dissipative/conservative Galerkin method using discrete partial derivatives for nonlinear evolution equations, J. Comput. Appl. Math. 218 (2008) 506–521.
[22] H. Lundmark, J. Szmigielski, Multi-peakon solutions of the Degasperis–Procesi equation, Inverse Prob. 19 (2003) 1241–1245.
[23] H. Lundmark, J. Szmigielski, Degasperis–Procesi peakons and the discrete cubic string, IMRP, Int. Math. Res. Pap. 2 (2005) 53–116.
[24] A. Degasperis, M. Procesi, Degasperis–Procesi equation, Scholarpedia 4 (2) (2009) 7318.
[25] W. Oevel, M. Sofroniou, Symplectic Runge–Kutta Schemes II: Classification of Symmetric Method, University of Paderborn Germany, preprint.
[26] R. Hixon, Nonlinear comparison of high-order and optimized finite-difference scheme, Int. J. Comput. Fluid Dyn. 13 (2000) 259–277.
[27] S.K. Lele, Compact finite difference schemes with spectral-like resolution, J. Comput. Phys. 103 (1992) 16–42.
[28] T. Nihei, K. Ishii, A fast solver of the shallow water equations on a sphere using a combined compact difference scheme, J. Comput. Phys. 187 (2003) 639–659.
[29] C.K.W. Tam, J.C. Webb, Dispersion-relation-preserving finite difference schemes for computational acoustics, J. Comput. Phys. 107 (1993) 262–281.
[30] G. Ashcroft, X. Zhang, Optimized prefactored compact schemes, J. Comput. Phys. 190 (2003) 459–477.
[31] B.P. Leonard, The ULTIMATE conservative difference scheme applied to unsteady one-dimensional advection, Comput. Methods Appl. Mech. Eng. 88 (1991) 17–74.
[32] P.C. Chu, C. Fan, A three-point combined compact difference scheme, J. Comput. Phys. 140 (1998) 370–399.